UNIVERSITY OF LEEDS

Article:
Kim, Y, Kim, YK, Kim, S et al. (2 more authors) (2017) Nanostructured potassium copper hexacyanoferrate-cellulose hydrogel for selective and rapid cesium adsorption. Chemical Engineering Journal, 313. pp. 1042-1050. ISSN 1385-8947

https://doi.org/10.1016/j.cej.2016.10.136

Nanostructured potassium copper hexacyanoferrate-cellulose hydrogel for selective and rapid cesium adsorption

Yonghwan Kim[a], Yun Kon Kim[a], Sungjun Kim[a], David Harbottle[b] and Jae W. Lee[a]*

[a]Department of Chemical and Biomolecular Engineering, Korea Advanced Institute of Science and Technology (KAIST), Daejeon 305-701, Republic of Korea

[b]School of Chemical and Process Engineering, University of Leeds, Leeds LS2 9JT, United Kingdom

KEYWORDS: Cesium adsorption, Immobilization, Potassium copper hexacyanoferrate, Cellulose hydrogel

Abstract

Potassium copper hexacyanoferrate (KCuHCF) was synthesized and immobilized in a cellulose-based hydrogel made of carboxymethyl cellulose (CMC) and hydroxyethyl cellulose (HEC) for the adsorption of cesium ions in aqueous solutions. The immobilization with the cellulose-based hydrogel facilitated the dispersion of nano-sized KCuHCF particles, showing the unprecedented adsorption capacity of the composite. In Cs^+ removal experiments, KCuHCF-cellulose hydrogel composites (HCF-gels) exhibited exceptional Cs^+ adsorption capacities (2.06-2.32 mmol g^{-1}) which was attributed to the presence of ion-exchangeable sites (COO^-Na^+) in the cellulose hydrogel. The HCF-gels also exhibited a rapid Cs^+ removal (90.1% removal for 0.15 mmol L^{-1} of Cs^+ in 1 h) with the uptake reaction kinetics expressed by a pseudo-second order kinetics model. Notably, the HCF-gels could adsorb Cs^+ selectively (>90%) in seawater containing 0.11 mmol L^{-1} Cs^+. Such specificity with fast kinetics is due to the high ion accessibility from the inherent nature of hydrogels and the highly dispersed KCuHCF nanoparticles in the composites.

1. Introduction

Due to the increased demand on world energy and the need to address global warming, nuclear power has been considered a sensible alternative to thermal power plants, generating about 10.6% of the world's electricity in 2013 [1]. Despite its efficient and carbon-free energy production, nuclear power is sometimes perceived as a threat because power production generates waste which requires treatment and continuous monitoring due to high levels of radioactivity, and the potential for uncontrolled release of radionuclides. For example, the incident at the Fukushima Daiichi nuclear power plant in 2011 caused large areas (soils and seawater) in Japan to become environmentally contaminated with radionuclides [2].

Among these radioelements, ^{137}Cs, a strong gamma emitter, is considered particularly problematic due to its long half-life (30.2 years) and transferability in the biosphere caused by its chemical similarity to potassium [3,4]. These radionuclides can be recovered using a range of diverse methods such as co-precipitation, evaporation/concentration, adsorption/ion-exchange, and chromatography [5]. However, in the case of a nuclear incident and a large scale release, those methods except for adsorption with ion-exchange are not suitable for the treatment of contaminated seawater due to the large volume of radioactive waste to be processed, and also the extremely low concentration of $^{137}Cs^{+}$ compared to competitive ions such as Na^{+}, K^{+} and Ca^{2+} [6,7]. Thus, it is desirable to develop ^{137}Cs selective adsorbents both for site operations and environmental decontamination.

A variety of cesium adsorbents including synthetic inorganic materials such as

zeolites [8], silicotitanates [9], and chalcogenides [10] have been considered due to their radiation stability and high thermal stability. However, their low Cs^+ selectivity limits their application in large-scale clean-ups. Recently mesoporous silica supported organic ligand adsorbents have been reported, but they are still in the development phase [11–13]. Alternatively, hexacyanoferrates containing transition metals have been widely studied, because the method of synthesis is relatively simple and cost-effective using a precipitation reaction between transition metals and hexacyanoferrate precursors [14]. Hexacyanoferrates possess a perovskite-like face-centered cubic structure with a channel size of 3.2 Å, so that hydrated ions including Cs^+, K^+ and NH^{4+} are able to permeate while larger hydrated ions such as Na^+ and Ca^{2+} are unable to exchange [15–17]. It has been reported that potassium copper hexacyanoferrate (KCuHCF) has high Cs^+ sorption capacity and selectivity compared to other metal hexacyanoferrates [18]. Despite the superb adsorption property and low production costs, direct use of KCuHCF as an adsorbent is not effective because its recovery following radionuclide adsorption is difficult due to its submicron size in the filtration process [17]. To overcome this drawback and use the adsorbent efficiently in large-scale processes, numerous studies have reported immobilization of sub-micron particles of metal hexacyanoferrates combined with various support materials [18,19].

In general, immobilization techniques can be categorized as either i) grafting onto support materials or ii) encapsulation using polymers. Since the former strategy immobilizes ion-exchangers onto the support surface, porous materials such as mesoporous silica [19,20] and carbon allotropes [21–24] are normally used. For the latter, ion-exchangers can be immobilized by encapsulation in polymer matrices such as chitin [3,18], alginate [21,25], and

polyacrylic acid [26]. With the encapsulation method, it is feasible to control the shape, such as bead and film formation, as well as to load considerable quantities of active ion-exchangers compared to the grafting method. Previous studies on polymer encapsulation [18,21] have focused on immobilization but not on enhancing the adsorption potential of the immobilizing composite material, because the supporting matrices generally showed low adsorption potentials.

Due to their abundant hydroxyl groups and mechanical strength, chemically modified celluloses have been studied [27]. Hydrogels based on carboxymethyl cellulose (CMC) and hydroxyethyl cellulose (HEC) crosslinked with citric acid (CA) have been reported as a superabsorbent because of its open-porous structure and hydrophilicity [28–30]. Because high water retention and diffusivity are important properties for immobilizing media, cellulose-based hydrogels can be an attractive option for the immobilization of KCuHCF particles.

Thus, this work introduces a facile, low-cost and effective method to immobilize KCuHCF using a cellulose-based hydrogel. Carboxylate anion (COO^-Na^+) sites in the CMC are the ion-exchangeable sites, so that Cs^+ adsorption capacity can be maintained after the KCuHCF particles are dispersed in the cellulose hydrogel network. In other words, a synergy between the hydrophilic, ion-exchangeable sites in the cellulose hydrogel and the high Cs^+ selectivity by the KCuHCF particles is desirable for effective Cs^+ remediation. Thus, the physicochemical characterization of the cellulose hydrogel, bulk KCuHCF, and HCF-gels was done to investigate the effect of their structures and chemical states on the adsorption

performance. Moreover, the Cs^+ adsorption performance was investigated in terms of the equilibrium capacity, kinetics, competitive adsorption with co-existing ions and material stability to determine the adsorption mechanism and its potential application in large-scale clean-ups.

2. Materials and methods

2.1. Materials

Potassium hexacyanoferrate ($K_4[Fe(CN)_6]\cdot 3H_2O$), sodium carboxymethyl cellulose (CMCNa, average molecular weight: 700,000 Da, degree of substitution (DS): 0.9, viscosity: 2500-6000 cP), hydroxyethyl cellulose (HEC, average molecular weight: 250,000 Da, DS: 1, viscosity: 80-125 cP), citric acid (CA) and untreated seawater were purchased from Sigma Aldrich. Copper sulfate ($CuSO_4\cdot 5H_2O$) was acquired from KANTO Chemical Co. Inc., and cesium chloride (CsCl, 99.9 % purity) was obtained from Alfa Aesar. All chemicals were used without further purification.

2.2. Synthesis of cellulose hydrogel and KCuHCF

The cellulose-based hydrogel film was synthesized by adopting a previously published method [28]. HEC and CMCNa at a 1:3 weight ratio were used as the cellulose backbone, and 20 wt% CA (based on the total weight of the two celluloses) was used as a crosslinking agent. It was reported that HEC, which is a nonionic polymer, is necessary to reduce the electrostatic repulsion between CMCNa to promote the formation of an open-porous structure [28,30]. First, 0.25 g HEC powder was dissolved in 100 mL deionized water

under magnetic stirring at room temperature for 1 h until a clear solution was observed. Then 0.75 g CMCNa powder was slowly added to the solution while avoiding the formation of particle aggregates. After 24 h, 0.2 g CA was added to this highly viscous and clear solution. The final solution was poured into a petri dish and dried at 30 ℃ in an oven for 24 h. Then, the sample was heated to 80 ℃ and kept at this temperature for 24 h to complete the crosslinking reaction. The obtained film was washed several times with deionized water and subsequently dried.

Bulk KCuHCF particles were synthesized in water by precipitation. First, 0.362 g $CuSO_4 \cdot 5H_2O$ and 0.507 g $K_4Fe(CN)_6$ were dissolved in two separate beakers with each 50 mL deionized water. Then the $K_4Fe(CN)_6$ solution was continuously added to the $CuSO_4$ solution dropwise under magnetic stirring for 4 h, until reaching a molar ratio of copper and iron equal to 1.2:1. The KCuHCF fine particles were separated via centrifugation and washed several times with deionized water. The final product was allowed to dry at 80 ℃ in an oven.

2.3. Synthesis of the KCuHCF-cellulose hydrogel composites

The schematic procedure to synthesize KCuHCF-cellulose hydrogel composites is shown in Fig. 1. First, 0.25 g HEC was dissolved in 50 mL deionized water with $CuSO_4 \cdot 5H_2O$ at different mass ratios of $CuSO_4$ to HEC equal to 1 (HCF-gel-1), 2 (HCF-gel-2), and 4 (HCF-gel-4). The solutions were gently agitated at room temperature for 1 h until a clear solution appeared. Then 0.75 g CMCNa powder was slowly added to each solution.

After 4 h, 50 mL $K_4Fe(CN)_6$ solution of different concentrations (26, 52, and 104 mmol L^{-1} for HCF-gel-1, 2, and 4, respectively), whose molar ratio between copper and iron was constant and equal to 1.2:1, was added dropwise. As a result, highly viscous brownish dispersions were obtained. After stirring for 18 h to get homogeneous dispersions, 0.2 g CA was added, and the resulting dispersions were poured into petri dishes followed by drying at 30 ℃ in an oven for 24 h. The samples were then heated to 80 ℃ and kept at this temperature for 24 h to complete the crosslinking reaction between HEC, CMCNa and CA. The final products were washed several times with deionized water to remove any unreacted materials and subsequently dried.

2.4. Characterization

The concentration of the metal elements was analyzed by inductively coupled plasma optical emission spectroscopy (ICP-OES, Agilent ICP-OES 720) after mineralization with a mixture of nitric acid and hydrochloric acid. Transmission electron microscopy (TEM) images were taken with a JEOL JEM-2100F at 200 kV. Before the TEM analysis, the HCF-gel-1 sample was ground and dissolved in 1 wt% acetic acid solution at 75 ℃ followed by drop-casting onto a nickel grid. Morphological characterization and elemental distribution were analyzed by scanning electron microscopy (SEM) using a Magellan 400 UHR-SEM at 1-3 kV coupled with energy dispersive X-ray (EDX) spectroscopy (OCTANE SUPER, EDAX). The X-ray diffraction (XRD) was conducted on a RIGAKU Ultima IV with Cu Kα (λ = 0.15418 nm) set at 40 kV and 40 mA. X-ray photoelectron spectroscopy (XPS) was performed with a Sigma probe (Thermo VG Scientific) to analyze the chemical bonds. The

XPS peaks were fitted with the Avantage software (Thermo VG package), and the binding energy was corrected with reference to C 1s at 284.5 eV. Fourier transform infrared (FT-IR) spectra were measured with an attenuated total reflectance (ATR) crystal on a Nicolet iS50 (400 – 4000 cm^{-1}). Thermogravimetric analyses to test thermal stability were done using a TG 209 F3 under a nitrogen atmosphere at a heating rate of 10 ℃ min^{-1} up to 600 ℃.

2.5. Cesium adsorption

Cesium (inactive cesium, ^{133}Cs) adsorption using the adsorbent samples was evaluated with a batch-shaking method. Each solid adsorbent was immersed in CsCl aqueous solutions with solution/adsorbent ratio of 2000 mL g^{-1}. The mixture was kept under agitation at 200 rpm and 20 ℃. After a fixed period of time, the adsorbent was isolated from the cesium solution using a syringe filter with a pore size of 0.45 μm. The initial and final cesium concentrations were measured with an inductively coupled plasma mass spectrometer (ICP-MS, Agilent ICP-MS 7700S).

The pH stability of HCF-gel-1 was evaluated by submerging 10 mg of HCF-gel-1 in 20 mL of 2 mmol L^{-1} Cs^+ solution of varying pH (2-11) for 24 h. HCl and NaOH were used to adjust the pH, and the initial pHs of the solution were measured with a S220 digital pH meter (Mettler Toledo). The final adsorbed Cs^+ concentrations were measured following the method previously discussed.

Cs^+ adsorption kinetics was studied by bringing into contact 100 mg of each adsorbent sample and 200 mL of 0.15 mmol L^{-1} Cs^+ solution for varying times up to 2200 mins. After a pre-determined time between 10 min and 36 h, 1 mL of the solution was extracted and the Cs^+ concentration was analyzed. The adsorbed cesium quantity, Q_t (mmol g^{-1}), and the removal efficiency, RE (%), were determined using the following relationships:

$$Q_t = (C_0 - C_t) \times V/m \quad (1)$$

$$\text{RE} = (C_0 - C_t)/C_0 \times 100\ (\%) \quad (2)$$

where C_0 (mmol L^{-1}) is the initial Cs^+ concentration, C_t (mmol L^{-1}) is the Cs^+ concentration after time t (min), V (L) is the volume of the solution, and m (g) is the mass of adsorbent.

For each adsorbent sample the adsorption isotherm was studied in Cs^+ solutions of varying concentrations after 24 h. 10 mg of the solid sample (adsorbent) was immersed in 20 mL Cs^+ solution of various concentrations between 0.04 mmol L^{-1} and 3 mmol L^{-1}. After 24 h of shaking, the solids were filtered, and the final Cs^+ concentrations (C_e, mmol g^{-1}) were evaluated.

Cs^+ selectivity was evaluated by submerging the adsorbents in seawater (untreated, Sigma Aldrich; Na^+: ~540 mmol L^{-1}, Mg^{2+}: ~60 mmol L^{-1}, K^+: ~12 mmol L^{-1}, Ca^{2+}: ~3.7 mmol L^{-1}) containing 0.004 mmol L^{-1} and 0.11 mmol L^{-1} Cs^+. 25 mg of the adsorbent sample was immersed in 50 mL seawater and shaken for 24 h. The final Cs^+ concentrations were measured, and the Cs^+ removal efficiencies were determined using equation (2).

3. Results and discussions

3.1. Textural characterization of KCuHCF-hydrogel composites

The chemical compositions of the KCuHCF particles in the HCF-gel samples were precisely evaluated with ICP-OES. Table 1 lists the metal content of each composite sample. Based on the collected data, the atomic ratios of K/Fe and Cu/Fe for HCF-gel-1, 2, and 4 were calculated to determine their chemical formulas. Taking into consideration the Cu/Fe ratios and the charge balance of each crystal, $K_2Cu_3[Fe(CN)_6]_2$ and $K_2CuFe(CN)_6$ co-exist. The content of the KCuHCF particles in each HCF-gel was estimated according to the metal content and chemical compositions. The mass fraction of KCuHCF increases with increasing amounts of the precursors of $CuSO_4 \cdot 5H_2O$ and $K_4Fe(CN)_6$.

The thermal stability and KCuHCF loading of HCF-gel-1 were investigated by the thermogravimetric analysis (TGA) (refer to Fig. S1 in the Supplementary Material (SM)). The initial weight loss of the samples, which occurred up to 150-200 ℃, was related to the elimination of absorbed and interstitial water molecules. The gradual weight reduction detected in the bulk KCuHCF from 150 ℃ was due to the structural decomposition and gas release including hydrogen cyanide [31]. The rapid weight loss in the range of 220-350 ℃ both in the cellulose hydrogel (46.6%) and HCF-gel-1 (30.0%) was attributed to polymer degradation. In the temperature range of 350-600 ℃, a gradual weight loss in the cellulose hydrogel was observed and it was attributed to further removal of oxygen functional groups. The weight loss in the HCF-gel-1 was due to the decomposition of both the cellulose

hydrogel and KCuHCF particles. A difference in the mass fraction between HCF-gel-1 and the cellulose hydrogel was equal to 18% at 600 ℃ which could be used to estimate the amount of KCuHCF particles in the composite. This result is comparable with the estimated value from the ICP-OES analysis (27.7%) which considered decomposed KCuHCF particles from 150 ℃.

Structural characterization of the adsorbent samples was done with TEM and SEM. As shown in Fig. 2(a), the TEM image of HCF-gel-1 revealed an even deposition of KCuHCF particles on the partially dissolved film which was pretreated with 1 wt% acetic acid for the effective specimen preparation. The well-dispersed KCuHCF particles were observed at higher magnification (Fig. 2(b)), and the particle size was measured to be approximately 10-12 nm. The morphology of the as-prepared samples was characterized by SEM. Prior to the SEM analysis, the cellulose hydrogel and HCF-gel samples were immersed in either deionized water (DI water) or a 2 mmol L^{-1} Cs^{+} solution followed by freeze-drying. Fig. 2(c) shows a representative SEM image of the cellulose hydrogel indicating a web-shaped macro-porous structure, and Fig. 2(d) is an image of the bulk KCuHCF showing a number of cubic-shaped particles with a size on the order of tens of nanometers. The analysis of HCF-gel-1 (Fig. 2(e)) also shows a web-shaped structure which is seen to be less ordered than the cellulose hydrogel (Fig. 2(c)). At higher magnification, shown in Fig. 2(f), the rough polymer surface of HCF-gel-1 and the undulations on the surface backbone are regarded as KCuHCF particles. From this morphological study, it was identified that the open structure of crosslinked cellulose could be maintained after the formation of the HCF-gel-1 composite

and that the KCuHCF particles were immobilized on the surface of the cellulose backbone. Immobilization using such a macro-porous hydrogel is advantageous for rapid access of cesium ions and confinement of a large amount of adsorbent particles compared to using other porous media [11,32]. The structures of the freeze-dried HCF-gel-2 and HCF-gel-4 were also investigated with the data shown in Fig. S2 (SM). The KCuHCF particle sizes were similar to those observed in HCF-gel-1; however, more particles were immobilized, weakening the network structures of the cellulose. Thus, it seems that an increased amount of KCuHCF particles inhibits cellulose crosslinking.

Moreover, the SEM-EDX analysis was done on HCF-gel-1 before and after Cs^+ adsorption. The distribution of K^+ in HCF-gel-1 before Cs^+ adsorption was shown in Fig. S3 (SM) to determine the distribution of the KCuHCF particles. These images indicate that the KCuHCF particles are uniformly distributed throughout the sample. Following Cs^+ adsorption, it was shown that Cs^+ was uniformly adsorbed, and the K+ concentration decreased slightly (Fig. S3). The atomic ratios of each metal based on Fe were listed in Table S1 (SM) because Fe hardly leached out from the composite during the adsorption process which was confirmed by ICP-MS. After Cs^+ adsorption, the atomic ratios of K (2.67) and Na (1.14) decreased to 0.85 and 0.59, respectively, and the ratio of Cs to Fe increased to 2.48. It should be noted that the adsorbed amount of Cs was comparable with the sum of decreased Na and K. Therefore, it suggests that the Cs^+ adsorption process is mostly by ion-exchange with K and Na in the HCF-gels.

3.2. Chemical characterization

X-ray diffraction (XRD) analyses of HCF-gel-1 were conducted to identify the phases of the adsorbent before and after Cs^+ adsorption. Fig. 3(a) shows the spectra of the bulk KCuHCF and HCF-gels before Cs^+ adsorption, confirming eight peaks around 2θ of 17.9° (200), 25.4° (220), 36.0° (400), 40.4° (420), 44.4° (422), 51.5° (440), 55.0° (600), and 58.4° (620). The spectrum shows that the as-prepared composites contain crystalline phases in the hydrogels which are consistent with those of the KCuHCF particles (Powder diffraction file, PDF No. 02-0383). Thus, it was ascertained that the KCuHCF particles were successfully immobilized. Moreover, the crystalline size (L, nm) of the KCuHCF in HCF-gel-1 was calculated using the Scherrer equation:

$$L = \frac{K \cdot \lambda}{\beta \cdot cos\theta} \quad (3)$$

where K is a dimensionless shape factor that varies with the crystal shape (taken as 0.94), λ is the X-ray wavelength (nm), β is the full-width at half-maximum height (FWHM, rad), and θ is the diffraction angle at the peak (rad).

The average particle size of the KCuHCF in HCF-gel-1 calculated from the major peaks at 17.9°, 25.4°, and 36.0° was equal to 9.8 nm, which is consistent with the TEM analysis (Fig. 2(b)), allowing for the fact that the Scherrer equation normally underestimates the crystal size compared with microscopic observation.[18] Following Cs^+ adsorption using HCF-gel-1 in 2 mmol L^{-1} Cs^+ solution (2000 mL g^{-1} ratio of solution to adsorbent for 24 h), the XRD peaks around 17.9°, 40.4°, 55.0° disappeared (Fig. 3(b)). The remaining peaks correspond well to those of CsCuHCF (PDF No. 24-0248). From this result, the ion-exchange

between K^+ and Cs^+ accompanied by the crystal phase transition is regarded as the main adsorption mechanism in HCF-gel-1.

Successful synthesis of the HCF-gels was confirmed by Fourier transform infrared spectroscopy (FT-IR). Fig. 3(c) shows the characteristic peaks of O-H stretching (3000-3400 cm^{-1}), C-H stretching (2850-3000 cm^{-1}), C=O stretching (1725-1735 cm^{-1}), glucose ring (1590-1610 cm^{-1}), C-O stretching (1000-1320 cm^{-1}) and C-C stretching (1300-1500 cm^{-1}) for the cellulose hydrogel and HCF-gel-1 [28,29]. Comparing HCF-gel-1 to the cellulose hydrogel, the C≡N stretching band at 2096 cm^{-1}, Fe^{2+}-C≡N- deformation band at 587 cm^{-1}, and -C≡N-Cu^{2+} deformation band at 484 cm^{-1} were additionally observed in the spectra [5,18], thus confirming the formation of the cellulose hydrogel-KCuHCF composite. The ester groups resulting from the crosslinking reaction were also investigated by comparing the FT-IR spectra of the reactants and products in the region of 1700-1800 cm^{-1} which represents carbonyl groups. As shown in Fig. 3(d), the peak at 1743 cm^{-1} in CA, which is the stretching band of carboxylic acid, moved to 1725-1730 cm^{-1} in the cellulose hydrogel and HCF-gel-1 after the crosslinking reaction between CA and cellulose at 80 ℃ [29]. The peak shift indicates the presence of ester groups, and the gelation from these groups formed water-stable films holding the KCuHCF particles.

XPS measurements were conducted to confirm the various carbon bonds and the Fe oxidation state in HCF-gel-1. As shown in the C 1s deconvolution spectra of HCF-gel-1 (Fig.

4(a)), four peaks centered at 283.83, 285.57, 287.26 and 288.33 eV were observed, corresponding to C-C/C-H, C-O, O-C-O and O=C-O groups, respectively. These are consistent with the FT-IR results and the existence of an ester group and carboxylate (COO^-) was also verified. Since the KCuHCF particles were mainly located inside the film of HCF-gel-1, the resolved peaks of HCF-gel-1 were obtained with a low intensity in the Fe 2p XPS spectra (Fig. 4(b)). The peaks centered at 708.25 eV and 721.15 eV were observed both in HCF-gel-1 and the bulk KCuHCF corresponding to Fe $2p_{3/2}$ of $[Fe(CN)_6]^{4-}$ and Fe $2p_{1/2}$ of Fe^{2+} state [22,33]. A small shoulder centered at 724.50 eV was detected in the bulk KCuHCF, which is attributed to the Fe $2p_{1/2}$ of Fe^{3+} state, indicating the partial oxidation of bulk particles. Nevertheless, this result confirms that most of the KCuHCF particles exist in the form of $K_xCu_y[Fe(CN)_6]_{4-x-2y}$, considering the oxidation state of Fe.

3.3. Effect of pH in solutions

The stability and adsorption performance of HCF-gel-1 were evaluated in Cs^+ solutions with varying pH. From Fig. 5, the amount of Cs adsorbed by HCF-gel-1 equals 1.5-1.9 mmol g^{-1}, and this is consistent over a wide pH range of 4-11. Even though the adsorption performance decreased in acidic conditions, the adsorption of Cs^+ by HCF-gel-1 in extremely acidic conditions (pH 2) still remained quite high and equal to 0.79 mmol g^{-1}. At low pH, the decrease in the Cs^+ adsorption capacity is related with a competition effect between H^+ and Cs^+ due to the protonation of the ion-exchange site. On the other hand, as the solution pH was adjusted to more basic conditions, the Cs^+ adsorption performance slightly increased, but the differences were not significant over the pH range 6-11. Such data show the application of HCF-gel-1 as an effective adsorbent of Cs^+ ions over a wide pH range, and considering this

consistency, subsequent Cs^+ adsorption experiments were conducted with dissolving CsCl in pure DI water.

3.4. Adsorption isotherm

To better understand the Cs^+ adsorption properties, equilibrium adsorption data were fitted with a Langmuir-isotherm to obtain information on the Cs^+ affinity, adsorption capacity, and adsorption mechanism. The adsorbed Cs^+ amount was calculated by comparing the initial and final concentrations of Cs^+ after 24 h of the adsorption time. Fig. 6(a) shows the Cs^+ adsorption equilibrium data of the cellulose hydrogel, bulk KCuHCF and HCF-gel-1 with Langmuir-isotherms fitted using the following equation:

$$Q_e = \frac{Q_m b C_e}{(1 + bC_e)} \quad (4)$$

where Q_e is the adsorbed Cs^+ quantity (mmol g^{-1}) at equilibrium, Q_m is a fitting parameter that represents the maximum adsorption capacity (mmol g^{-1}), b is a fitting parameter that represents the affinity coefficient (L $mmol^{-1}$), and Ce is the Cs^+ concentration of the aqueous phase at equilibrium (mmol L^{-1}).

Langmuir-isotherm parameters are listed in Table 2. The adsorption capacity of HCF-gel-1 was found to be 2.06 mmol g^{-1}, which was intermediate to the cellulose hydrogel and bulk KCuHCF. It is worthwhile to note that the cellulose hydrogel itself adsorbed Cs^+ with a high value of Q_m (1.97 mmol g^{-1}). The ICP-MS data after Cs^+ adsorption by the cellulose hydrogel, which quantifies the amount of released Na^+ and adsorbed Cs^+, validated the ion-exchange between Cs^+ and Na^+ occurring at the COO^-Na^+ sites in the hydrogel structure

(Table S2 in SM). For HCF-gel-1, the abundance of the ion-exchangeable sites in the cellulose hydrogel backbone enables more Cs^+ ions to be adsorbed. As a result, the Cs^+ adsorption capacity of HCF-gel-1 was highly retained after immobilization, even though the content of the KCuHCF particles in HCF-gel-1 was only about 27 wt%. The adsorption equilibrium results for HCF-gel-2 and HCF-gel-4 are shown in Fig. 6(b) and Table 2, and Q_m and b increased with an incremental amount of KCuHCF particles. The adsorption capacity of HCF-gel-4 (2.32 mmol g^{-1}) is one of the highest values among the studies for the immobilization of metal hexacyanoferrates (Table 3). Such high adsorption capacities can be important when they are used for high level waste in terms of the volume reduction of radioactive waste.

Recognizing the fact that there could be different binding sites in the HCF-gels, which are the KCuHCF particles and the carboxylates of the cellulose, Langmuir adsorption was not appropriate to describe the Cs^+ adsorption mechanism of the HCF-gels. Hence, to investigate the difference in the binding energy, the dual-site Langmuir equation was introduced as follows:

$$Q_e = \frac{Q_{m,1} b_1 C_e}{(1 + b_1 C_e)} + \frac{Q_{m,2} b_2 C_e}{(1 + b_2 C_e)} \quad (5)$$

where Ce is the Cs^+ concentration of the aqueous phase at equilibrium (mmol L^{-1}), $Q_{m,1}$ and b_1 are the maximum adsorption capacity (mmol g^{-1}) and the affinity coefficient (L $mmol^{-1}$) on the first kind of binding sites, respectively, and $Q_{m,2}$ and b_2 are similar parameters on the second kind of binding sites.

As can be seen from Table 2, the correlation coefficient (R^2) values were increased when fitted with the dual-site Langmuir equation, reflecting the validity of considering different kinds of binding sites. The gap between the sets of ($Q_{m,1}$, b_1) and ($Q_{m,2}$, b_2) verifies the multiple adsorption sites of each sample.

3.5. Adsorption kinetics

Adsorption kinetics was studied to evaluate the required time to remove Cs^+ and to understand how the cellulose hydrogel could contribute to the fast removal of Cs^+. Fig. 7(a) shows the Cs^+ removal efficiency of the cellulose hydrogel, bulk KCuHCF, and HCF-gel-1 at various time intervals. All samples reached equilibrium within a few hours of contact. HCF-gel-1 removed 90% of the 0.15 mmol L^{-1} Cs^+ within approximately 1 h, and both HCF-gel-1 and bulk KCuHCF removed >99% of Cs^+ after 4 h. However, the cellulose hydrogel could not remove all the Cs^+, due to the low affinity of Cs^+ to the carboxylate (COO^-Na^+) sites in the cellulose. To quantify the initial rapid adsorption, adsorption data were analyzed using a pseudo-second-order kinetics model as follows:

$$\frac{t}{Q_t} = \frac{1}{k_2 Q_e^2} + \frac{t}{Q_e} \quad (6)$$

where Q_t is the adsorbed Cs quantity (mmol g^{-1}) at time t (min), Q_e is the adsorption capacity at equilibrium (mmol g^{-1}), and k_2 is a parameter that represents the rate constant for the pseudo-second-order model (g $mmol^{-1}$ min^{-1}).

As shown in Table 4, the rate constants (k_2) of the cellulose hydrogel, bulk KCuHCF,

and HCF-gel-1 were 0.517, 0.0584 and 0.144 g $mmol^{-1}$ min^{-1}, respectively. This trend corresponds to the order of the adsorbed Cs^+ amount by each sample in the first 10 min. The behavior is attributed to the structure accessible by Cs^+ and the high hydrophilicity by the anionic functional groups (COO^-). Therefore, in the HCF-gel-1 sample, the structural and chemical properties of the cellulose hydrogel contributed to the rapid Cs^+ removal while maintaining the adsorption capacity of KCuHCF. The adsorption kinetics of HCF-gel-2 and HCF-gel-4 were also investigated (Fig. S4 in SM), and all the HCF-gels could adsorb Cs^+ quickly with the rate constant (k_2) of each composite having comparable values.

3.6. Competitive cesium removal

The effect of competing ions on the adsorption of Cs^+ was evaluated using a seawater solution. From a practical standpoint, it is important to selectively remove small amounts of Cs^+ from a background of coexisting cations such as Na^+, K^+, Mg^{2+}, and Ca^{2+}. 0.004 and 0.11 mmol L^{-1} Cs^+ was added to untreated seawater, and the removal efficiency and distribution coefficient (K_d) for each adsorbent are shown in Fig. 7(b) and Table 5, respectively. K_d (mL g^{-1}) is used to evaluate the Cs^+ selectivity and is given by

$$K_d = \frac{V(C_0 - C_e)}{mC_e} \quad (7)$$

where C_0 and C_e are the initial and equilibrium concentrations of Cs^+ (mmol L^{-1}), respectively, V is the volume of the Cs^+ solution (mL), and m is the mass of the adsorbent (g).

The K_d values for HCF-gels and bulk KCuHCF in seawater were calculated to be of

the order of 10^4 - 10^5 mL g^{-1}. These K_d values in seawater were comparable with those determined by conducting adsorption studies in DI water. In terms of the cesium removal performance, all adsorbents removed more than 90% of Cs^+ (up to 98.3% with HCF-gel-2) confirming that the effect of coexisting ions on the removal of Cs^+ was negligible. Interestingly, the cellulose hydrogel could not remove Cs^+ in seawater (data not shown). This indicates that the selectivity of the carboxylates over Cs^+ was not sufficient in conditions with extremely high concentrations of coexisting cations. Nevertheless, the removal efficiencies of all the HCF-gels were similar to that of the bulk KCuHCF particles. It seems that the accessibility of the Cs^+ ions to KCuHCF particles did not decrease due to the swelling property and hydrophilicity of the cellulose hydrogel. In addition, the dispersion of the KCuHCF particles in the HCF-gels possibly contributed to the high Cs^+ removal efficiency in seawater condition, although they contain smaller amount of KCuHCF particles.

4. Conclusions

KCuHCF particles were effectively immobilized by crosslinking functionalized celluloses with citric acid to recover Cs^+ from contaminated aqueous solutions. The Cs^+ adsorption performance of the HCF-gels exceeded that of individual cellulose hydrogels and bulk KCuHCF particles. The HCF-gel-1 sample was observed to remove >99% of Cs^+ (0.15 mmol L^{-1}) within 4 h maintaining its adsorption stability over a wide pH range of 4 to 11. The maximum Cs^+ adsorption capacity of the HCF-gels ranges from 2.06 to 2.32 mmol g^{-1}, which is one of the highest adsorption capacities reported to date. Such increased adsorption capacity is due to the additional ion-exchangeable sites of carboxylates in the cellulose hydrogel, because the cellulose hydrogel also showed potential for Cs^+ adsorption. The dual-

site Langmuir equation validated the two different adsorption sites. HCF-gel-4, containing more KCuHCF particles, showed comparable adsorption kinetics but a slightly larger adsorption capacity than that of HCF-gel-1. In addition, HCF-gels were able to remove trace amounts of Cs^+ (0.004 - 0.11 mmol L^{-1}) from seawater selectively (>90%) as well as bulk KCuHCF. This adsorption performance is related to the well-dispersed KCuHCF nanoparticles in the composite and the high ion accessibility in the cellulose hydrogel due to the well-maintained open-porous structure.

Acknowledgements

The authors are grateful for the financial support from the UKKorea Joint Research Program through NRF grants (NRF-2015M2A7A1000219) funded by the Ministry of Science, ICT, and Future Planning. D. Harbottle acknowledges the support of Engineering and Physical Sciences Research Council grant number EP/M026426/1.

REFERENCES

[1] Key World Energy Statistics, International Energy Agency, 2015, https://www.iea.org/publications/freepublications/publication/KeyWorld_Statistics_2015.pdf, (accessed June 2016).

[2] T.J. Yasunaria, A. Stohl, R.S. Hayano, J.F. Burkhart, S. Eckhardt, T. Yasunarie, Cesium-137 deposition and contamination of Japanese soils due to the Fukushima nuclear accident, Proc. Natl. Acad. Sci. 108 (2011) 19530–19534. doi:10.1073/pnas.1112058108.

[3] C. Vincent, Y. Barré, T. Vincent, J.M. Taulemesse, M. Robitzer, E. Guibal, Chitin-Prussian blue sponges for Cs(I) recovery: From synthesis to application in the treatment of accidental dumping of metal-bearing solutions, J. Hazard. Mater. 287 (2015) 171–179. doi:10.1016/j.jhazmat.2015.01.041.

[4] H.-M. Yang, K.-W. Lee, B.-K. Seo, J.-K. Moon, Copper Ferrocyanide-Functionalized Magnetic Nanoparticles for the Selective Removal of Radioactive Cesium, J. Nanosci. Nanotechnol. 15 (2015) 1695–1699. doi:10.1166/jnn.2015.9313.

[5] A. Nilchi, R. Saberi, M. Moradi, H. Azizpour, R. Zarghami, Adsorption of cesium on copper hexacyanoferrate-PAN composite ion exchanger from aqueous solution, Chem. Eng. J. 172 (2011) 572–580. doi:10.1016/j.cej.2011.06.011.

[6] R.O. Abdel Rahman, H.A. Ibrahium, Y.T. Hung, Liquid radioactive wastes treatment: A review, Water (Switzerland). 3 (2011) 551–565. doi:10.3390/w3020551.

[7] S.J. Datta, W.K. Moon, D.Y. Choi, I.C. Hwang, K.B. Yoon, A novel vanadosilicate with hexadeca-coordinated Cs^+ ions as a highly effective Cs^+ remover, Angew.

Chemie - Int. Ed. 53 (2014) 7203–7208. doi:10.1002/anie.201402778.

[8] P.K. Sinha, P.K. Panicker, R. V. Amalraj, V. Krishnasamy, Treatment of radioactive liquid waste containing caesium by indigenously available synthetic zeolites: A comparative study, Waste Manag. 15 (1995) 149–157. doi:10.1016/0956-053X(95)00014-Q.

[9] H. Liu, A. Yonezawa, K. Kumagai, M. Sano, T. Miyake, Cs and Sr removal over highly effective adsorbents ETS-1 and ETS-2, J. Mater. Chem. A. 3 (2015) 1562–1568. doi:10.1039/C4TA06170E.

[10] M.J. Manos, M.G. Kanatzidis, Highly Efficient and Rapid Cs^+ Uptake by the Layered Metal Sulfide $K_{2x}Mn_xSn_{3-x}S_6$ (KMS-1), J. Am. Chem. Soc. 131 (2009) 6599–6607. doi:10.1021/ja900977p.

[11] M.R. Awual, Ring size dependent crown ether based mesoporous adsorbent for high cesium adsorption from wastewater, Chem. Eng. J. 303 (2016) 539–546. doi:10.1016/j.cej.2016.06.040.

[12] M.R. Awual, Y. Miyazaki, T. Taguchi, H. Shiwaku, T. Yaita, Encapsulation of cesium from contaminated water with highly selective facial organic-inorganic mesoporous hybrid adsorbent, Chem. Eng. J. 291 (2016) 128–137. doi:10.1016/j.cej.2016.01.109.

[13] M.R. Awual, T. Yaita, T. Taguchi, H. Shiwaku, S. Suzuki, Y. Okamoto, Selective cesium removal from radioactive liquid waste by crown ether immobilized new class conjugate adsorbent, J. Hazard. Mater. 278 (2014) 227–235. doi:10.1016/j.jhazmat.2014.06.011.

[14] C. Loos-Neskovic, S. Ayrault, V. Badillo, B. Jimenez, E. Garnier, M. Fedoroff, et al.,

Structure of copper-potassium hexacyanoferrate (II) and sorption mechanisms of cesium, J. Solid State Chem. 177 (2004) 1817–1828. doi:10.1016/j.jssc.2004.01.018.

[15] C.D. Wessells, R.A. Huggins, Y. Cui, Copper hexacyanoferrate battery electrodes with long cycle life and high power., Nat. Commun. 2 (2011) 550. doi:10.1038/ncomms1563.

[16] R.Y. Wang, B. Shyam, K.H. Stone, J.N. Weker, M. Pasta, H.W. Lee, et al., Reversible Multivalent (Monovalent, Divalent, Trivalent) Ion Insertion in Open Framework Materials, Adv. Energy Mater. 5 (2015) 1401869. doi:10.1002/aenm.201401869.

[17] M.A. Olatunji, M.U. Khandaker, H.N.M.E. Mahmud, Y.M. Amin, Influence of adsorption parameters on cesium uptake from aqueous solutions- a brief review, RSC Adv. 5 (2015) 71658–71683. doi:10.1039/C5RA10598F.

[18] T. Vincent, C. Vincent, Y. Barré, Y. Guari, G. Le Saout, E. Guibal, Immobilization of metal hexacyanoferrates in chitin beads for cesium sorption: synthesis and characterization, J. Mater. Chem. A. 2 (2014) 10007. doi:10.1039/c4ta01128g.

[19] T. Sangvanich, V. Sukwarotwat, R.J. Wiacek, R.M. Grudzien, G.E. Fryxell, R.S. Addleman, et al., Selective capture of cesium and thallium from natural waters and simulated wastes with copper ferrocyanide functionalized mesoporous silica, J. Hazard. Mater. 182 (2010) 225–231. doi:10.1016/j.jhazmat.2010.06.019.

[20] J. Causse, A. Tokarev, J. Ravaux, M. Moloney, Y. Barré, A. Grandjean, Facile one-pot synthesis of copper hexacyanoferrate nanoparticle functionalised silica monoliths for the selective entrapment of 137Cs, J. Mater. Chem. A. 2 (2014) 9461. doi:10.1039/c4ta01266f.

[21] H. Yang, H. Li, J. Zhai, L. Sun, Y. Zhao, H. Yu, Magnetic prussian blue/graphene oxide nanocomposites caged in calcium alginate microbeads for elimination of cesium ions from water and soil, Chem. Eng. J. 246 (2014) 10–19. doi:10.1016/j.cej.2014.02.060.

[22] H. Yang, L. Sun, J. Zhai, H. Li, Y. Zhao, H. Yu, In situ controllable synthesis of magnetic Prussian blue/graphene oxide nanocomposites for removal of radioactive cesium in water, J. Mater. Chem. A. 2 (2014) 326–332. doi:10.1039/c3ta13548a.

[23] L. Wang, M. Feng, C. Liu, Y. Zhao, S. Li, H. Wang, et al., Supporting of Potassium Copper Hexacyanoferrate on Porous Activated Carbon Substrate for Cesium Separation, Sep. Sci. Technol. 44 (2009) 4023–4035. doi:10.1080/01496390903183253.

[24] A.A. Kadam, J. Jang, D.S. Lee, Facile synthesis of pectin-stabilized magnetic graphene oxide Prussian blue nanocomposites for selective cesium removal from aqueous solution, Bioresour. Technol. 216 (2016) 391–398. doi:10.1016/j.biortech.2016.05.103.

[25] J. Jang, D.S. Lee, Enhanced adsorption of cesium on PVA-alginate encapsulated Prussian blue-graphene oxide hydrogel beads in a fixed-bed column system, Bioresour. Technol. 218 (2016) 294–300. doi:10.1016/j.biortech.2016.06.100.

[26] H. Yang, H. Li, J. Zhai, H. Yu, In situ growth of Prussian blue nanocrystal within Fe^{3+} crosslinking PAA resin for radiocesium highly efficient and rapid separation from water, Chem. Eng. J. 277 (2015) 40–47. doi:10.1016/j.cej.2015.04.047.

[27] Y. Habibi, Key advances in the chemical modification of nanocelluloses, Chem. Soc.

Rev. 43 (2014) 1519–1542. doi:10.1039/c3cs60204d.

[28] C. Demitri, R. Del Sole, F. Scalera, A. Sannino, G. Vasapollo, A. Maffezzoli, et al., Novel superabsorbent cellulose-based hydrogels crosslinked with citric acid, J. Appl. Polym. Sci. 110 (2008) 2453–2460. doi:10.1002/app.28660.

[29] M.G. Raucci, M.A. Alvarez-Perez, C. Demitri, D. Giugliano, V. De Benedictis, A. Sannino, et al., Effect of citric acid crosslinking cellulose-based hydrogels on osteogenic differentiation, J. Biomed. Mater. Res. - Part A. 103 (2015) 2045–2056. doi:10.1002/jbm.a.35343.

[30] C. Chang, B. Duan, J. Cai, L. Zhang, Superabsorbent hydrogels based on cellulose for smart swelling and controllable delivery, Eur. Polym. J. 46 (2010) 92–100. doi:10.1016/j.eurpolymj.2009.04.033.

[31] M. Pasta, C.D. Wessells, N. Liu, J. Nelson, M.T. McDowell, R.A. Huggins, et al., Full open-framework batteries for stationary energy storage, Nat. Commun. 5 (2014) 3007. doi:10.1038/ncomms4007.

[32] M.R. Awual, T. Yaita, Y. Miyazaki, D. Matsumura, H. Shiwaku, T. Taguchi, A Reliable Hybrid Adsorbent for Efficient Radioactive Cesium Accumulation from Contaminated Wastewater., Sci. Rep. 6 (2016) 19937. doi:10.1038/srep19937.

[33] X. Wang, Q. Xiang, B. Liu, L. Wang, T. Luo, D. Chen, et al., TiO_2 modified FeS nanostructures with enhanced electrochemical performance for lithium-ion batteries, Sci. Rep. 3 (2013) 2007. doi:10.1038/srep02007.

[34] C.Y. Chang, L.K. Chau, W.P. Hu, C.Y. Wang, J.H. Liao, Nickel hexacyanoferrate multilayers on functionalized mesoporous silica supports for selective sorption and

sensing of cesium, Microporous Mesoporous Mater. 109 (2008) 505–512. doi:10.1016/j.micromeso.2007.05.057.

[35] L. Vrtoch, M. Pipíška, M. Horník, J. Augustín, J. Lesný, Sorption of cesium from water solutions on potassium nickel hexacyanoferrate-modified Agaricus bisporus mushroom biomass, J. Radioanal. Nucl. Chem. 287 (2011) 853–862. doi:10.1007/s10967-010-0837-5.

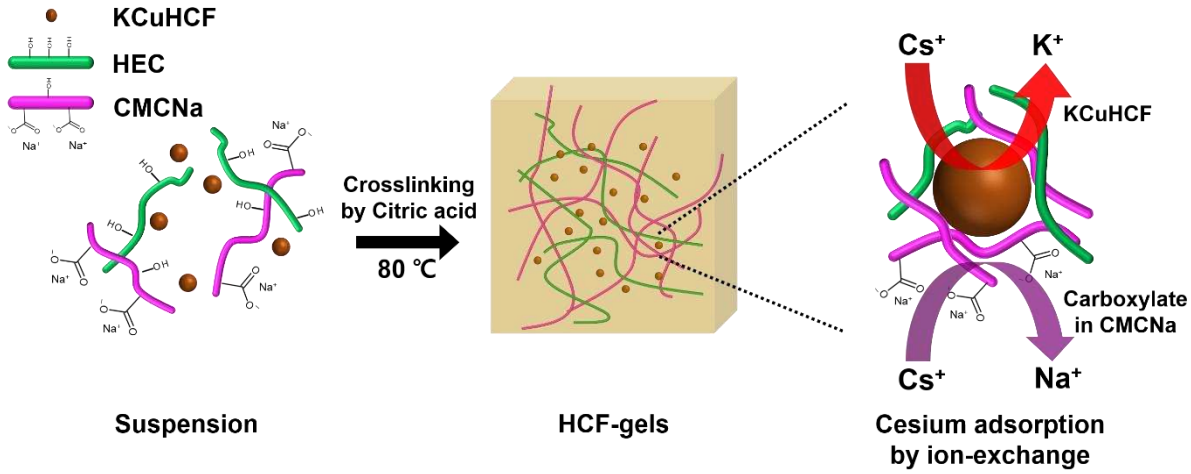

Fig. 1. Representation of synthesis and cesium adsorption of HCF-gels.

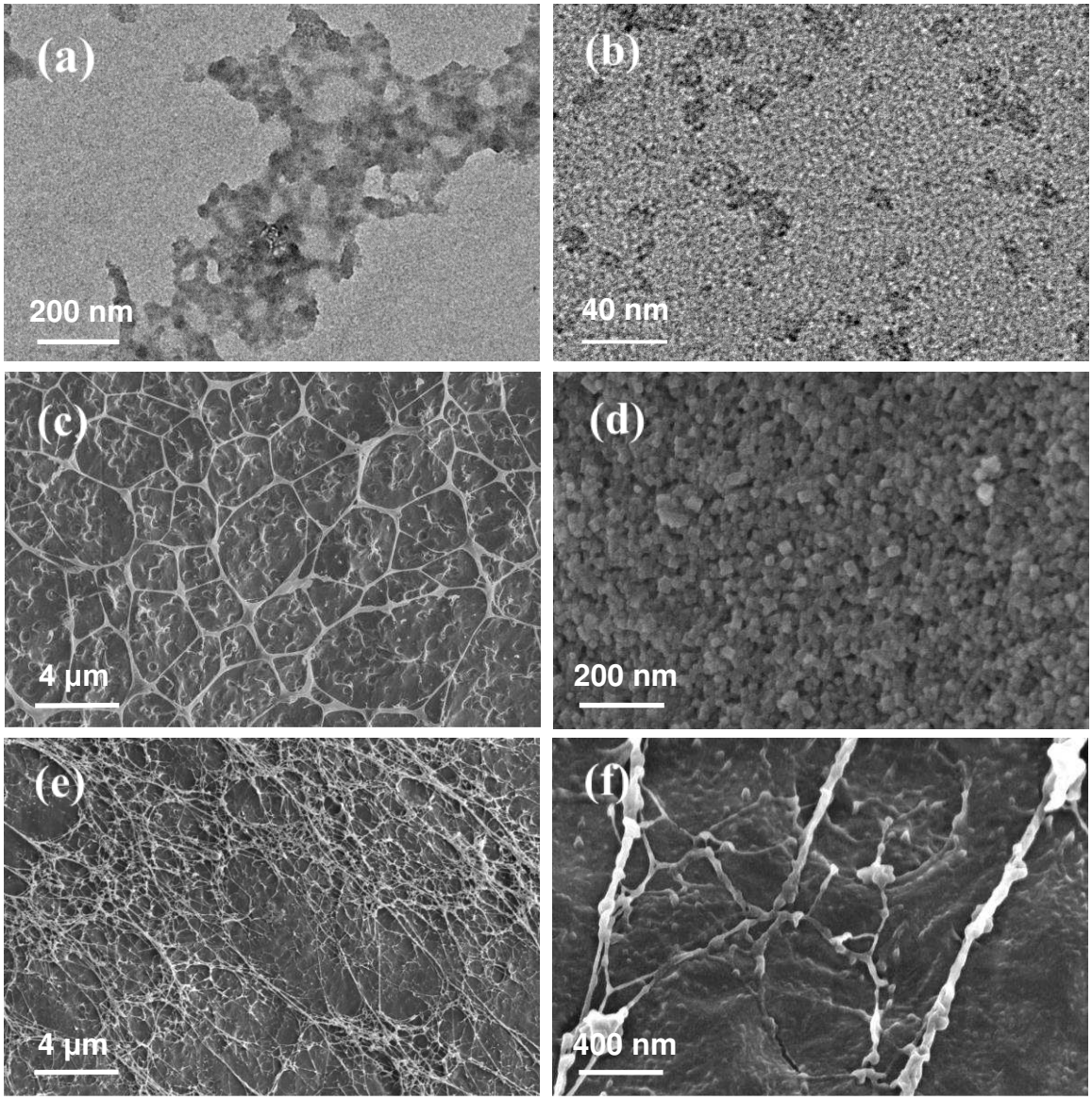

Fig. 2. TEM images of (a) HCF-gel-1 (b) HCF-gel-1 (higher magnification), and SEM images of (c) cellulose hydrogel (d) bulk KCuHCF (e) HCF-gel-1 (d) HCF-gel-1 (higher magnification).

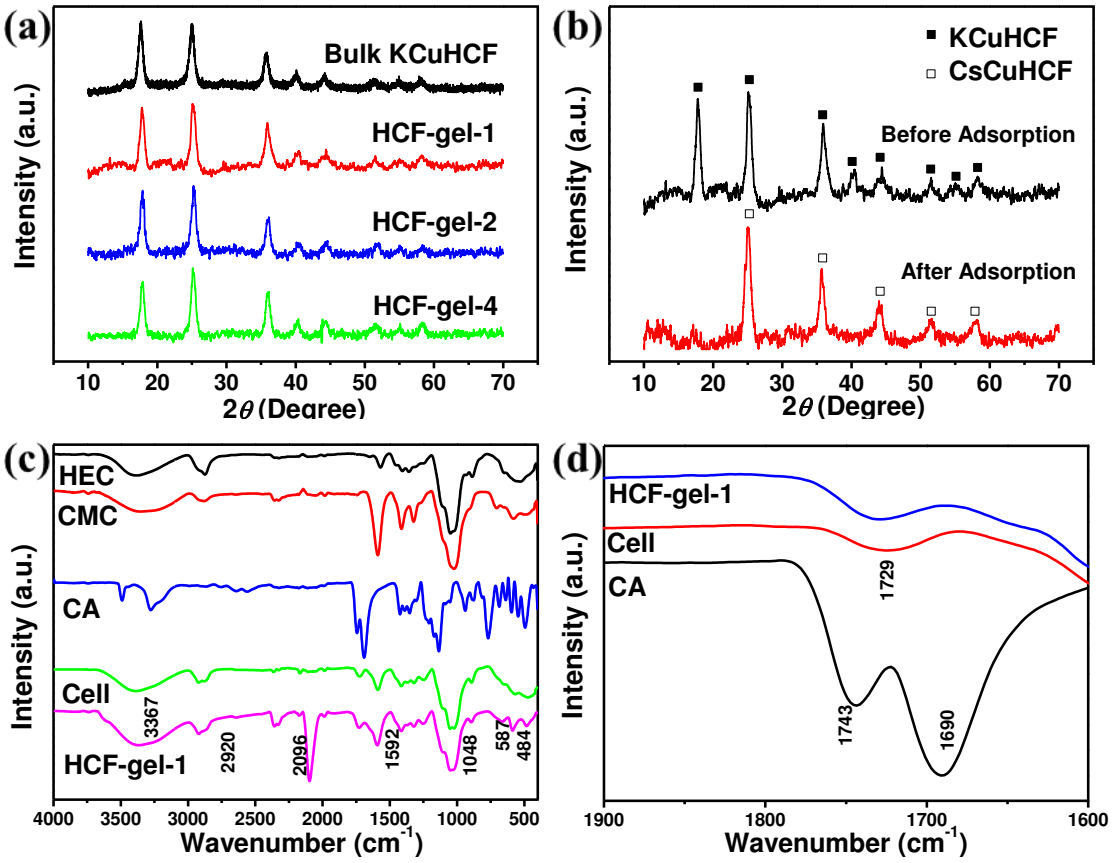

Fig. 3. XRD patterns of (a) bulk KCuHCF and HCF-gels, (b) HCF-gel-1 before and after Cs^{+} adsorption (contact with 2 mmol L^{-1} Cs^{+} solution for 24 h; V/m ~ 2L/g)) and FT-IR spectra of (c) HEC, CMC, CA, cellulose hydrogel, and HCF-gel-1, (d) HCF-gel-1, cellulose hydrogel, and CA in the region of 1600-1800 cm^{-1}.

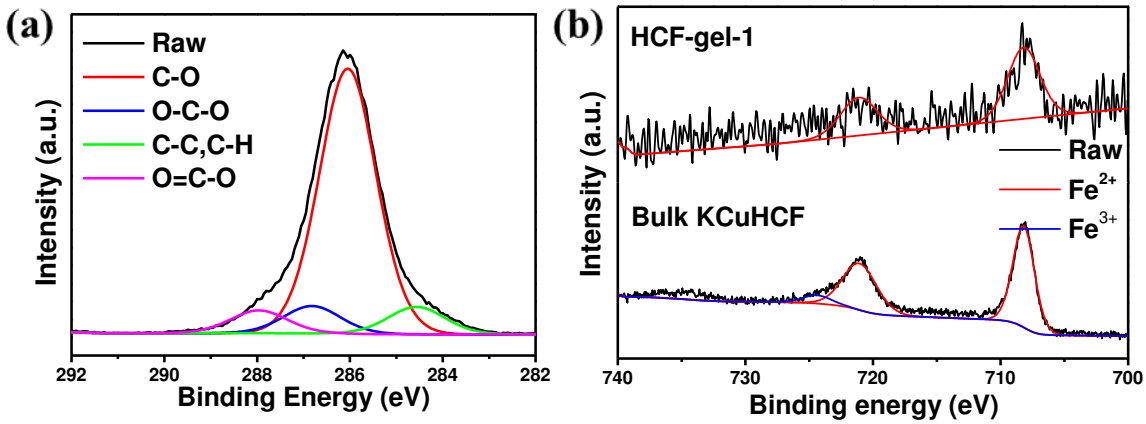

Fig. 4. XPS spectra of (a) C 1s peak for HCF-gel-1 and (b) Fe 2p peaks for HCF-gel-1 and bulk KCuHCF.

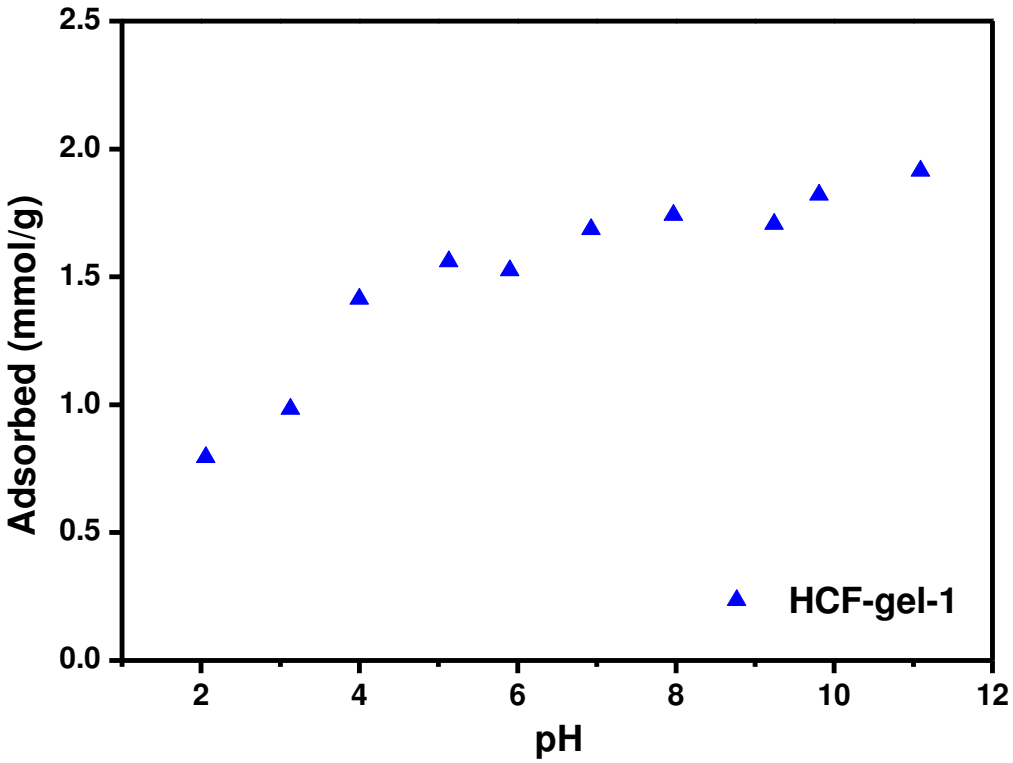

Fig. 5. Cs^{+} adsorption data of HCF-gel-1 varying initial pH (C_0 = 2 mmol L^{-1}).

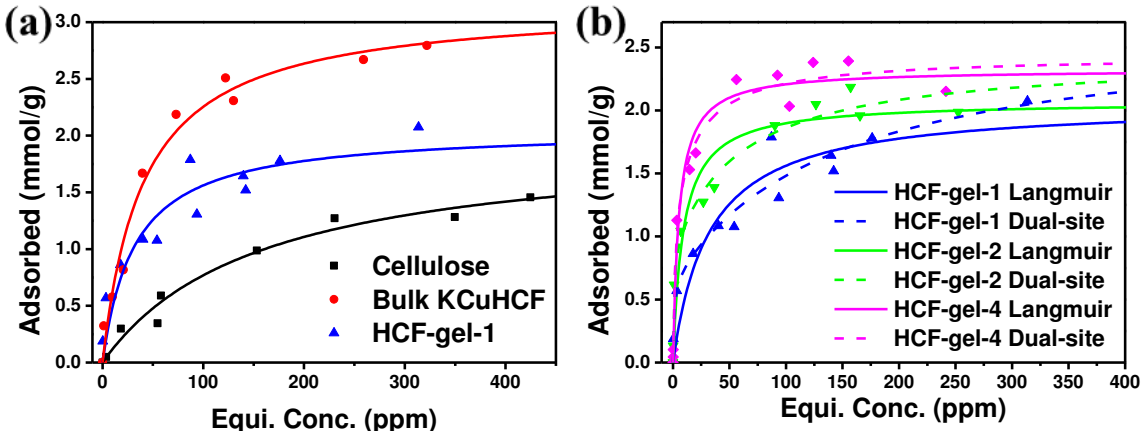

Fig. 6. Cs^{+} adsorption isotherms of (a) cellulose hydrogel, bulk KCuHCF, and HCF-gel-1 with Langmuir fitting curves and (b) HCF-gels with fitting curves by Langmuir equation and dual-site Langmuir equation.

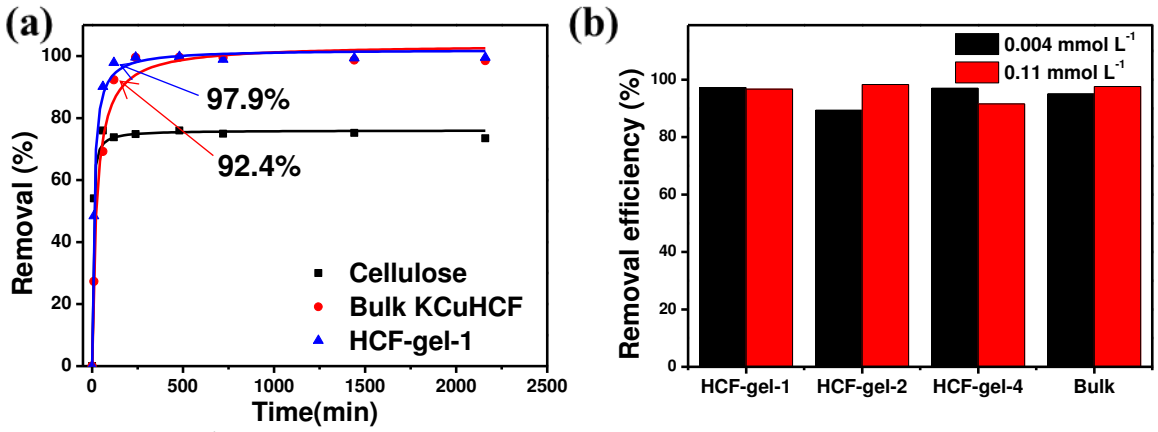

Fig. 7. (a) Cs^{+} uptake kinetics with fitting curve by pseudo-second order rate equation (C_0 = 20 ppm), (b) Cs+ removal efficiencies of each adsorbent in seawater (C_0 = 0.004, 0.11 mmol L^{-1})

Table 1 Metal content and chemical composition of each HCF-gels analyzed by ICP-OES.

Sample	K (mmol/g)	Cu (mmol/g)	Fe (mmol/g)	Form	Content (wt%)
HCF-gel-1	1.2183	1.0063	0.7798	$K_{1.56}Cu_{1.29}Fe(CN)_6$	27.6928
HCF-gel-2	1.7875	1.3971	1.1087	$K_{1.61}Cu_{1.26}Fe(CN)_6$	39.3753
HCF-gel-4	2.2623	2.1136	1.6383	$K_{1.38}Cu_{1.29}Fe(CN)_6$	57.0140

Table 2 Cs^+ adsorption parameters obtained from fitting with Langmuir equation and dual-site Langmuir equation.

Sample	Langmuir			Dual-site Langmuir				
	Q_m (mmol g^{-1})	b (L $mmol^{-1}$)	R^2	$Q_{m,1}$ (mmol g^{-1})	b_1 (L $mmol^{-1}$)	$Q_{m,2}$ (mmol g^{-1})	b_2 (L $mmol^{-1}$)	R^2
Cellulose hydrogel	1.9748	0.8479	0.9749					
Bulk KCuHCF	3.1691	3.2733	0.9799					
HCF-gel-1	2.0604	4.1558	0.8985	2.0333	0.9117	0.6610	151.3452	0.9429
HCF-gel-2	2.0701	14.6602	0.9288	1.5415	2.3417	0.8852	214.8807	0.9786
HCF-gel-4	2.3249	24.8683	0.9756	1.0950	6.0749	1.3402	69.38177	0.9762

Table 3 Cs^+ adsorption capacities from other studies related to immobilization of metal hexacyanoferrates.

Co-metal	Support	Adsorption capacity (mmol Cs/g composite)	Reference
Cu	HEC+CMC	2.06-2.32	This work
Cu	Silica	0.13	[19]
Cu	PAN	0.19	[5]
Cu	Chitin	0.89	[18]
Fe	Graphene oxide/Fe_3O_4	0.42	[22]
Fe	Poly(acrylic acid)	0.55	[26]
Ni	Silica	1.69	[34]
Ni	Biomass	1.07	[35]

Table 4 Cs^+ adsorption kinetics parameters obtained from fitting with pseudo-second order rate equation.

Sample	k_2 (g $mmol^{-1}$ min^{-1})	Q_m (mmol g^{-1})	R^2
Cellulose hydrogel	0.5172	0.5246	0.9932
Bulk KCuHCF	0.0584	0.7101	0.9864
HCF-gel-1	0.1442	0.6981	0.9950
HCF-gel-2	0.0834	0.6623	0.9918
HCF-gel-4	0.1091	0.6706	0.9909

Table 5 Distribution coefficient (K_d) values of adsorbents

Sample	K_d (mL/g)*	K_d (mL/g)**	K_d (mL/g)***
Cellulose hydrogel	4.637×10^3		
Bulk KCuHCF	2.276×10^5	9.250×10^4	8.445×10^4
HCF-gel-1	3.808×10^4	1.811×10^5	6.092×10^4
HCF-gel-2	2.460×10^4	4.315×10^4	1.182×10^5
HCF-gel-4	1.587×10^5	1.620×10^5	2.172×10^4

***** K_d for DI water solution (0.07 mmol L^{-1} of Cs^+)

****** K_d for seawater solution (0.004 mmol L^{-1} of Cs^+)

******* K_d for seawater solution (0.11 mmol L^{-1} of Cs^+)